AGU PUBLICATIONS

JGR

Journal of Geophysical Research: Atmospheres

RESEARCH ARTICLE

10.1002/2014JD021808

Key Points:
- In the extratropics, the DT frequency increases with the stability of the TIL
- Upward vertical motion increases with DT frequency and TIL stability
- Increase in DT frequency over the Pacific Ocean coincides with WCB formation

Correspondence to:
T. R. Peevey,
t.peevey@fz-juelich.de

Citation:
Peevey, T. R., J. C. Gille, C. R. Homeyer, and G. L. Manney (2014), The double tropopause and its dynamical relationship to the tropopause inversion layer in storm track regions, *J. Geophys. Res. Atmos.*, *119*, 10,194–10,212, doi:10.1002/2014JD021808.

Received 24 MAR 2014
Accepted 23 JUN 2014
Accepted article online 27 JUN 2014
Published online 8 SEP 2014

The double tropopause and its dynamical relationship to the tropopause inversion layer in storm track regions

T. R. Peevey[1,2], J. C. Gille[2,3], C. R. Homeyer[2], and G. L. Manney[4,5]

[1]Institut für Energie and Klimaforschung: Stratosphäre (IEK-7), Forschungszentrum Jülich, Jülich, Germany, [2]Atmospheric Chemistry Division, National Center for Atmospheric Research, Boulder, Colorado, USA, [3]Center for Limb Atmospheric Sounding, University of Colorado at Boulder, Boulder, Colorado, USA, [4]NorthWest Research Associates, Socorro, New Mexico, USA, [5]New Mexico Institute of Mining and Technology, Socorro, New Mexico, USA

Abstract Using High Resolution Dynamic Limb Sounder observations and ERA-Interim reanalysis this study demonstrates that the warm conveyor belt (WCB) is a mechanism responsible for the relationship between the double tropopause (DT) and the tropopause inversion layer (TIL), a relationship recently suggested in the literature based on idealized model simulations of baroclinic disturbances. Using these data sets, spatial and temporal characteristics of the DT-TIL relationship are examined over a 3 year period, 2005–2008. In the extratropics, results from satellite data show that as the TIL increases in strength, so does the frequency of the DT, regardless of season or hemisphere. The inverse relationship is found in the tropics. Using only DT profiles, zonal composites of wind, relative vorticity, and temperature from reanalysis data show that as the TIL increases in strength, the upper tropospheric circulation switches from cyclonic to anticyclonic, and the upward vertical motion increases. This result suggests the WCB as a mechanism since it is on the anticyclonic side of the jet and is characterized by the movement of tropical air poleward and upward from the surface. To verify this relationship, the vertical and horizontal development of a synoptic-scale baroclinic system is analyzed over a 4 day period. Results show the equatorward extension of the polar tropopause, and thus the formation of the DT, due to the strengthening of the TIL in the region of vertical motion associated with the WCB. Moreover, this result suggests that air movement within the DT could originate from high latitudes when associated with a baroclinic disturbance.

1. Introduction

The tropopause separates the troposphere and the stratosphere, two layers of the atmosphere that are chemically, dynamically, and thermally distinct [e.g., *Holton et al.*, 1995; *Hoinka*, 1997; *Kunz et al.*, 2011a]. The characteristics of the tropopause and the surrounding region, the upper troposphere and lower stratosphere (UTLS), are important for multiple reasons. For example, the tropopause acts as a barrier that tends to suppress stratosphere-troposphere exchange (STE), so that to quantify midlatitude STE, we first need to understand the structure and variability of the tropopause [e.g., *Randel et al.*, 2007a; *Kunz et al.*, 2011a, 2011b]. Furthermore, the tropopause is located in a region of minimum temperatures, which can be used as an indicator of climate change since it is sensitive to changes in the concentration of radiatively active species in the UTLS [*Gettelman et al.*, 2011, and references therein].

Above the tropopause there is a very stable thermal structure called the tropopause inversion layer (TIL). It is a layer of stable air that varies between 1 and 3 km thick, is a persistent atmospheric feature, preferentially forms above anticyclonic circulations, and is better identified in tropopause based coordinates [e.g., *Wirth*, 2003; *Birner et al.*, 2002; *Birner*, 2006; *Randel et al.*, 2007b; *Grise et al.*, 2010]. In the tropics the TIL is most stable in the winter and the least stable in the summer due to the seasonal cycle of the Brewer-Dobson circulation [*Birner*, 2010] and equatorial planetary waves [*Grise et al.*, 2010]. In the extratropics the seasonal cycle of the TIL is the opposite, such that the stability maximum is reached in the summer and the minimum in the winter. The increase in stability of the extratropical TIL during the polar summer has thus far been shown to result primarily from an increase in radiative forcing from water vapor increases at the tropopause [*Randel et al.*, 2007b; *Kunz et al.*, 2009; *Birner*, 2010]. During the winter the intraseasonal variability in the stratospheric polar vortex [*Grise et al.*, 2010] and the Brewer-Dobson circulation are the primary drivers [*Birner*, 2010]. Equatorward of those regions but poleward of the subtropical jet, the TIL exhibits a

similar seasonal cycle that weakens when moving equatorward. In this region the TIL seasonal cycle has been shown to be the product of multiple mechanisms such as adiabatic warming above the tropopause due to the Brewer-Dobson circulation [*Birner*, 2010], upper tropospheric cyclonic and anticyclonic circulations [*Wirth*, 2003; *Randel et al.*, 2007b; *Wirth and Szabo*, 2007; *Homeyer et al.*, 2010], and the radiative effects of water vapor [*Kunz et al.*, 2009].

In midlatitudes the higher tropical tropopause can overlap the lower polar tropopause, forming the characteristic break in the thermal tropopause along the subtropical jet and the double tropopause (DT), the latter of which is the focus of this study. The DT was first documented in the 1930s [*Bjerknes and Palmen*, 1937], and further studied in the 1950s [*Kochanski*, 1955; *Danielsen*, 1959] using soundings and in the 1970s using aircraft observations [*Shapiro*, 1978, 1980]. A more recent modeling study by *Wirth* [2001] showed, using balanced dynamics, that the DT can form when either a negative or positive potential vorticity (PV) anomaly is introduced into the background UTLS atmosphere, thus highlighting dynamical aspects of the DT. However, even though the DT can form above both cyclonic and anticyclonic circulations [see *Wirth*, 2001], there is a clear tendency for the DT to form above strong cyclonic circulations in the real atmosphere, which could be a result of the destabilizing effect of the cyclonic circulation in the lower stratosphere [*Randel et al.*, 2007a] and/or a result of forming on the cyclonic side of the subtropical jet due to localized warming at the tropopause by the descending branch of the Brewer-Dobson circulation that underlies a cool region near the poleward edge of the tropical tropopause formed by the ascending branch of the Brewer-Dobson circulation [*Birner*, 2010].

DTs have been shown to occur more frequently above strong upper tropospheric cyclonic circulations and during the winter season due to seasonal changes in the strength of atmospheric circulations [*Randel et al.*, 2007a; *Wernli and Schwierz*, 2006; *Manney et al.*, 2014], form preferentially on the poleward (cyclonic) side of the subtropical jet and are coincident with the characteristic tropopause break [*Randel et al.*, 2007a; *Pan and Munchak*, 2011; *Peevey et al.*, 2012; *Manney et al.*, 2014], and can be associated with a decrease in the concentration of ozone in the lower stratosphere suggesting enhanced transport from the tropical troposphere [*Randel et al.*, 2007a; *Pan et al.*, 2009]. Case studies of individual events have shown that DTs associated with poleward transport events are formed via Rossby wave breaking [e.g., *Pan et al.*, 2009; *Homeyer et al.*, 2011; *Ungermann et al.*, 2013]. These Rossby wave breaking events can cause the DT structure and the associated tropical tropospheric air mass to separate from the tropical reservoir and irreversibly mix with the background air in the lower stratosphere. Recent long-term studies of DT propagation patterns have further revealed their association with Rossby wave breaking, which is particularly frequent over the eastern Pacific Ocean and thus may be a common occurrence over certain regions [e.g., *Castanheira and Gimeno*, 2011; *Peevey et al.*, 2012; *Manney et al.*, 2014]. However, even though the above observational studies have shown that Rossby wave breaking and poleward transport can account for a significant fraction of DT events, DTs are also frequently found in the absence of Rossby wave breaking [e.g., *Biondi et al.*, 2012].

The scientific significance of the DT stems from the combination of its residence in the UTLS and its connection to atmospheric structures associated with STE [*Pan et al.*, 2009]. As stated previously, the DT is found to occur during Rossby wave breaking events and is most frequent during the winter, a season for intense weather systems. Both of these are known mechanisms for STE; however, DTs are most frequently associated with poleward wave breaking events [e.g., *Pan et al.*, 2009; *Homeyer et al.*, 2011; *Ungermann et al.*, 2013] that can transport low ozone air into the lower stratosphere. This air, once mixed in with the background atmosphere, would decrease stratospheric ozone and consequently cool the stratosphere/troposphere, which could counteract some of the warming due to global warming [*Fahey et al.*, 2008]. As the frequency of DTs increase due to climate change, as shown by *Castanheira et al.* [2009], this feedback could intensify. However, some questions still remain that leave the exact level of importance of the DT and its use as a marker for STE open to discussion. For example, years with high DT frequency are not necessarily years of frequent irreversible mixing events [*Olsen et al.*, 2010], so the question of how often DTs are associated with irreversible STE events is still present. Additionally, as the jet shifts poleward due to climate change poleward wave breaking has been shown to reduce [*Barnes and Hartmann*, 2012], which would reduce the ability of DT associated with poleward wave breaking to counteract global warming.

Climatological studies of the DT have found that there is a strong spatial coincidence between DT frequency and storm track regions of cyclogenesis [*Schmidt et al.*, 2006; *Añel et al.*, 2008; *Peevey et al.*, 2012], which are located over the Pacific and Atlantic oceans in both the Southern and Northern Hemisphere [*Wernli and*

Schwierz, 2006; *Holton and Hakim*, 2013]. This spatial relationship prompted many recent studies of DTs and baroclinic waves since extratropical storms form from developing baroclinic waves and are associated with STE events that impact the chemical composition of air masses in the UTLS and at the surface [e.g., *Stohl et al.*, 2003]. *Castanheira et al.* [2009] found that as the baroclinicity in the UTLS increases, a potential outcome of climate change [e.g., *Garcia and Randel*, 2008; *Randel et al.*, 2009], so does the DT frequency. Subsequent studies showed that the meridional extent of the DT is strongly correlated with baroclinic Rossby waves [*Castanheira and Gimeno*, 2011] along with upwelling in the tropics and the frequency of low ozone lamina in the lower stratosphere [*Castanheira et al.*, 2012].

One study in particular, *Wang and Polvani* [2011], examined the LC1/2 baroclinic life cycles using idealized model simulations. The LC1/2 life cycles are diagnosted using potential temperature on PV surfaces (2 PVU) by *Thorncroft et al.* [1993] and defined as having anticyclonic/cyclonic behavior such that the anticyclonic/LC1 behavior is characterized by backward tilting, thinning troughs that are advected anticyclonically and equatorward and the cyclonic/LC2 behavior by forward tilting, broadening troughs that wrap up cyclonically and poleward. Some of the differences between the LC1/2 life cycles include the following: the LC1(2) life cycle is associated with broad and weak jets (narrow and strong jets) [*Esler and Haynes*, 1999], is more prevalent during El Niño/cold phase (La Niña/warm phase) [*Shapiro et al.*, 2001], and results in more air being transported into the stratosphere from the boundary layer but with less mixing (larger stratosphere to troposphere transport and overall more mixing for either direction of transport due to deep cyclonic vortices) [*Polvani and Esler*, 2007]. The baroclinic life cycle study by *Wang and Polvani* [2011] found that the DT would spontaneously form only in the presence of the extratropical TIL and that as the lapse rate/strength of the TIL decreased/increased so did the number of DTs. This is interesting because, as stated previously, the TIL tends to form above anticyclonic circulations and is strongest in the extratropics during the summer, both characteristics not exhibited by the DT. This unexpected positive correlation between the DT and the TIL and the general importance of understanding STE pathways within the UTLS directly motivate this study. The broader or more indirect motivation for this work comes from the fact that although modeling and observational studies have documented several processes that can be associated with the DT, as presented above, the relationship between the TIL and the DT is not known.

We evaluate the dynamical relationship between the DT and the TIL using satellite observations and reanalysis data. The data sets utilized in this study and the methods used to identify the DT and the TIL are presented in the first two sections. Section 4 presents an analysis of the relationship between the DT and the TIL and identifies the dynamical mechanisms that are potentially responsible. These results are discussed and related to previous work in section 5. A brief conclusion is presented in the final section.

2. Data

2.1. HIRDLS V6 Level 2 Profiles

The High Resolution Dynamic Limb Sounder (HIRDLS) is one of four instruments on board the NASA EOS-Aura satellite. The Aura satellite was launched on 15 July 2004 into a Sun-sychronous orbit with a period of 99 min and an altitude of 705 km. At this altitude the satellite circles the globe ~14.5 times per day, resulting in orbits with a longitudinal separation of 24.75°. Along track, the latitudinal separation between profiles is 75–100 km or ~1°. HIRDLS is a 21 channel limb-scanning radiometer that observes in the infrared (between 6 and 18 μm or ~550 and 1670 cm^{-1}), allowing measurement of emissions from Earth's atmosphere both day and night [*Gille et al.*, 2008, and references therein]. Between ~63°S and ~80°N the HIRDLS instrument measures approximately 5500 profiles per day and crosses the equator twice per orbit, once at approximately midnight and once at approximately 3 P.M. (local time).

Data collection began on 21 January 2005 and ended on 17 March 2008 when the instrument failed; for this work, data are analyzed beginning on 29 January 2005, after the instrument settled into a stable state. HIRDLS temperature data are calculated from the CO_2 bands between 15 and 17 μm and are the only products used from the HIRDLS data set since this study focuses on the DT and the TIL, both thermally defined structures. The temperature product has been shown to agree well with radiosondes, lidar (Mauna Loa and Table Mountain), alternative satellite observations, and model analyses, both in its vertical and horizontal structure [*Gille et al.*, 2008; *Gille and Gray*, 2011]. Additionally, HIRDLS has been shown to measure the thermal atmosphere down to scales of ~2 km wavelengths in the vertical, i.e., ~1 km fine-scale features, equivalent to the FORMOSAT-3/Constellation Observing System for Meteorology, Ionosphere, and Climate

[*Gille and Gray*, 2011; *Wright et al.*, 2011]. Further information on instrument specifications and the temperature product, including validation, can be found in *Gille et al.* [2008] and *Gille and Gray* [2011]. Information on the HIRDLS retrieval algorithm can be found in *Khosravi et al.* [2009].

These properties highlight the key attributes that make HIRDLS an effective instrument for analyzing the UTLS, a region that has been difficult to measure with previous satellites because of fine-scale structures [e.g., *Lahoz et al.*, 2007; *Olsen et al.*, 2010]. Additionally, HIRDLS, relative to other currently available observations, generates daily data sets with high global data density and high along-track horizontal resolution that enable detailed analyses of meridionally extensive structures such as the DT [e.g., *Peevey et al.*, 2012].

2.2. GEOS5.1.0

Version 5 of the Goddard Earth Observing System Model (GEOS5) system was developed by NASA's Global Modeling and Assimilation Office to support Aura and other satellites that are part of the Earth Observing Systems (EOS) program. GEOS5 is an assimilation system that uses a combination of model forecasts and observations to generate reanalysis products (see *Rienecker et al.* [2008] for detailed information). GEOS5 is used instead of other reanalysis products since it was generated for the NASA EOS program and has good vertical resolution in the UTLS. Multiple versions of GEOS5 are available; however, version 5.1.0 is used in this study to calculate the location of the subtropical jet (see section 4.1) instead of version 5.2.0 since it spans a 5 year period (2003–2008) that overlaps the HIRDLS mission (2005–2008). The version presented here is also used for HIRDLS a priori data, i.e., the initial guess in satellite retrieval algorithms. GEOS5 data are generated as either 6-hourly time-averaged fields time stamped at the center of the averaging window or instantaneous fields with no time averaging. Both data sets are available every 6 h at 00Z, 06Z, 12Z, and 18Z.

For this study the 6-hourly time-averaged fields are used instead of the instantaneous fields since they are available on the native model levels, for which the vertical resolution is ~1 km in the UTLS [*Rienecker et al.*, 2008] (72 levels from the surface to 0.01 hPa). In the horizontal, the resolution is 0.5° latitude by 0.67° (2/3°) longitude.

2.3. European Center for Medium-Range Weather Forecasting ERA-Interim

In this study HIRDLS observations are supplemented with data from the European Reanalysis (ERA-Interim) Version 2.0 so that the dynamical state of the atmosphere can be assessed. The ERA-Interim data product runs from 1979 to present and is the latest global reanalysis product from the European Center for Medium-Range Weather Forecasting (ECMWF) [*Berrisford et al.*, 2011; *Dee et al.*, 2011]. This product is used over the Modern-Era Retrospective Analysis for Research and Applications (MERRA), a reanalysis product produced using the GEOS5 system, because of a low bias in DT frequency detection relative to ERA-Interim and HIRDLS (not shown), which could be a result of inaccurate upper tropospheric temperature profiles either due to incorrect humidity levels in the upper troposphere [*Chung et al.*, 2013] and/or the shallow vertical extent of the tropical maximum diabatic heating profile found in MERRA [*Wright and Fueglistaler*, 2013]. ERA-Interim is available on a horizontal Gaussian latitude-longitude grid of 0.75° × 0.75° at 6 h increments (00, 6, 12, and 18 UTC). In the vertical, ERA-Interim offers two different grid options: 37 levels on pressure surfaces or 60 levels on model surfaces. In this study both surfaces are utilized. For the composites shown in section 4.2 the 37 level vertical grid is used, and the original horizontal grid is linearly interpolated onto a 1.5° × 1.5° latitude-longitude grid between 10°N and 80°N. The 37 pressure levels are unevenly spaced in the UTLS; however, the resolution around the tropopause is approximately 1 km. This is sufficient for finding small-scale features in the UTLS [*Kunz*, 2009; *Kunz et al.*, 2009], and additionally, it is nearly equivalent to the vertical resolution of HIRDLS. Above 150 hPa the vertical resolution degrades to greater than 1 km, which is compensated for using the technique presented in section 3.1. For the case study model, levels on the original horizontal grid are used since the computational cost is not as high, and more importantly, subtle features will be more clearly captured since the vertical resolution is approximately 1 km throughout the UTLS.

3. Methodology

3.1. Double Tropopause Algorithm

In this study the World Meteorological Organization thermal definition [*World Meteorological Organization*, 1957] of the DT is used. The definition is stated as follows: (1) the first tropopause is defined as the lowest level at which the lapse rate γ (defined as $-dT/dz$) decreases to 2°C km^{-1} or less, provided that the average lapse rate between this level and all higher levels within 2 km does not exceed 2°C km^{-1}, and

(2) if above the first tropopause the average lapse rate between any level and all higher levels within 1 km exceeds 3°C km^{-1}, then a second tropopause is defined under the same criterion as under (1). The second tropopause may be either within or above the 1 km layer discussed in step 2. For this study K km^{-1} is used instead of C km^{-1}, since these units are equivalent for lapse rate calculations and temperature data are given in Kelvin.

The DT algorithm is only used above altitudes of 5 km (or ~550 hPa) for all data sets to avoid false DT detections from near-surface temperature inversions. The algorithm also stops at the second tropopause and does not search for additional tropopauses since they are not the focus of this study. In this study, the HIRDLS data set is not cloud cleared since previous work has illustrated that characteristics of the DT are not affected by the presence of clouds [e.g., *Peevey*, 2013]. For the ERA-Interim 37 level data set, additional steps are required since the vertical resolution is 1 km at the tropopause but greater than 1 km above 150 hPa, the region of the second tropopause. To compensate for this, each profile is interpolated onto 0.2 km altitude intervals using a cubic spline (comparable results are achieved with a linear interpolation). This is only done to obtain the location of the DT; after the DT is found, the original temperature data are used and all other variables, such as wind, relative vorticity, etc, are also used on their original vertical levels. This interpolation is not needed for the ERA-Interim data set with 60 vertical levels due to its 1 km vertical resolution.

3.2. Locating the Tropopause Inversion Layer

Above the thermally defined first tropopause there is often a region of high static stability called the tropopause inversion layer (TIL), which is identified using the square of the Brunt Väisälä frequency as follows:

$$N^2 = \frac{g}{\theta}\frac{\partial \theta}{\partial z} = \frac{g}{T}\left(\frac{\partial T}{\partial z} + \Gamma_d\right) \quad (1)$$

$$\theta = T\left(\frac{P_0}{P}\right)^{\frac{R}{c_p}} \quad (2)$$

where T is temperature, z is altitude, θ is potential temperature, g is the gravitational constant, R is the gas constant for dry air, c_p is the specific heat capacity at a constant pressure, and Γ_d is the dry adiabatic lapse rate (9.8°K km^{-1}). In the troposphere the static stability is low ($N^2 \approx 1 \times 10^{-4}$ s^{-2}), and in the stratosphere it is high ($N^2 \approx 4 \times 10^{-4}$ s^{-2}) [e.g., *Birner*, 2006; *Randel et al.*, 2007b; *Kunz*, 2009; *Grise et al.*, 2010]. Upon entering the stratosphere, the stability increases dramatically and then gradually decreases to typical stratospheric levels over the next few kilometers. This layer with a maximum in static stability is the TIL, and it can contain stability values as high as 8×10^{-4} s^{-2} [e.g., *Birner*, 2006; *Randel et al.*, 2007b; *Grise et al.*, 2010].

In this study, the TIL is found by isolating the level of maximum stability within the first 3 km above the first tropopause using equation (1). Thus, TIL information shown in this study is reported at one layer, where the maximum static stability occurs. Lapse rate information, calculated by differencing the temperature between the level of maximum stability and the next level immediately above, is also recorded at the level of maximum stability since this was the parameter used by *Wang and Polvani* [2011] to measure the strength of the TIL. Moreover, this will be the parameter used to indicate TIL strength throughout this document. Three kilometers is chosen for the altitude range because the average depth of the TIL is approximately 2 km ±1 km [*Birner et al.*, 2002; *Grise et al.*, 2010]. For the stability calculation, altitude and potential temperature data are used from each data set, and if the potential temperature is not provided, it is calculated using equation (2). Evidence showing that this simple method accurately characterizes the TIL is briefly presented in section 4.1 and further discussed in Appendix A.

3.3. Referencing the Subtropical Jet

The subtropical jet is used to separate different groups of DTs for two reasons: (1) the majority of DTs are found along and poleward of the subtropical jet as illustrated by case studies and climatological analyses of DT/jet relationships [*Schmidt et al.*, 2006; *Pan et al.*, 2009; *Peevey et al.*, 2012; *Manney et al.*, 2014] and (2) storm tracks are linked to the planetary-scale flow, which includes upper tropospheric jet streams such as the subtropical jet [*Chang et al.*, 2002]. Therefore, to separate DTs related to storm tracks from other DTs, the subtropical jet is used as the point of reference for all plots shown in section 4.1.

The subtropical jet is located using the method of *Manney et al.* [2011] (called "maximum wind" method hereinafter), which locates the subtropical and polar jet cores and identifies their characteristics using meteorological analyses. Using this technique, all jet cores between the 100 hPa and 400 hPa pressure surfaces

Table 1. Mean Tropopause Heights (km)

	Eastern Pacific Ocean		Western Pacific Ocean	
Tropopause	DJF[a]	JJA[b]	DJF	JJA
First	10.50	11.03	9.05	10.77
Second	16.33	15.78	15.73	15.74

[a]December-January-February.
[b]June-July-August.

are identified. When the wind speed exceeds 40 m s^{-1} along a longitude line, an upper tropospheric jet is found to exist. The boundary of the jet is where the wind speed drops below 30 m s^{-1}. If another maximum is found within the 30 m s^{-1} contour, then additional tests are applied to determine if there are two separate jet cores. In the present work the above steps are applied to the GEOS5 data set after it has been interpolated to HIRDLS longitude points. For further details on the technique, see *Manney et al.* [2011]. After the subtropical jet is found, the DT and TIL data are placed into latitude bins such that positive bins are poleward of the jet and negative bins are equatorward of the jet.

The subtropical jet was also identified using two other methods to validate the above method. First, the latitude of the maximum wind on the 200 hPa surface was found for each HIRDLS orbit starting from the equator, since the core of the subtropical jet tends to be near that pressure surface [e.g., *Strong and Davis*, 2006; *Randel et al.*, 2007a; *Schiemann et al.*, 2009]. Second, the regions equatorward, around, and poleward of the subtropical jet were isolated using the altitude of the first tropopause such that all profiles with a tropopause above 14 km are considered to be in the tropics, all profiles with a tropopause below 12 km in the extratropics and all profiles between 12 and 14 km in the transition region [e.g., *Pan and Munchak*, 2011].

In addition to the above, only second tropopauses that are at pressures greater than 70 hPa are included in the DT-TIL analysis in section 4.1 since tropopause pressure distributions show that the number of second tropopauses drops off dramatically when the pressure decreases below ~70 hPa, both in the tropics and extratropics, and all secondary tropopauses are found at pressures less than 250 hPa [*Peevey*, 2013]. As a result, this limit removes profiles with false DT identifications from the analysis.

3.4. Vertical Scaling

This section describes a vertical scaling algorithm that is applied to the ERA-Interim data before generating the zonal composites shown In section 4.2. The purpose of the technique is to ensure that structures within the DT, i.e., between the first and second tropopause, are not smoothed out or lost in the averaging. This is done by setting the altitude of the first tropopause and second tropopause to the average for that region and season (see Table 1), and then adjusting the original tropopause levels to these fixed levels, thus stretching or compressing each profile individually. The steps of the algorithm are shown below and are executed in the order presented from top to bottom:

$$z > 0 \;: z_r = z_{r\_trop1} + (z - z_{trop1}) \tag{3}$$

$$z_{trop1} < z \le z_{trop2} \;: z_r = \left(\left(z_{r\_trop2} - z_{r\_trop1} \right) * \left(\frac{z - z_{trop1}}{z_{trop2} - z_{trop1}} \right) \right) + z_{r\_trop1} \tag{4}$$

$$z > z_{trop2} \;: z_r = z_{r\_trop2} + (z - z_{trop2}) \tag{5}$$

where z is the original profile, z_{trop1} and z_{trop2} are equal to the altitude of the first and second tropopause in the original profile, z_r represents the new profile, z_{r_trop1} represents the first tropopause in the new profile and is equal to the mean value of the first tropopause for the region, and z_{r_trop2} represents the second tropopause of the new profile and is equal to the mean value of the second tropopause for the region (see Table 1 for exact values). Equation (3), which shifts the whole profile vertically such that z_{trop1} equals z_{r_trop1}, is first applied to the whole original profile. Next, equation (4) is used, but only on levels between the first and second tropopause of the original profile such that the original profile is stretched or compressed so that z_{trop2} equals z_{r_trop2}. Equation (5) is applied to all levels above z_{trop2} in the original profile, resulting in those levels shifting vertical until z_{trop2} equals z_{r_trop2}. This method can result in negative altitude values near what was the surface in the original profile; however, that is not a significant concern since this study focuses on the UTLS. The final result is the profile z_r with the same number of levels as the original profile, z, but with slightly different altitude values such that the relative location of features between the first and second tropopause are preserved.

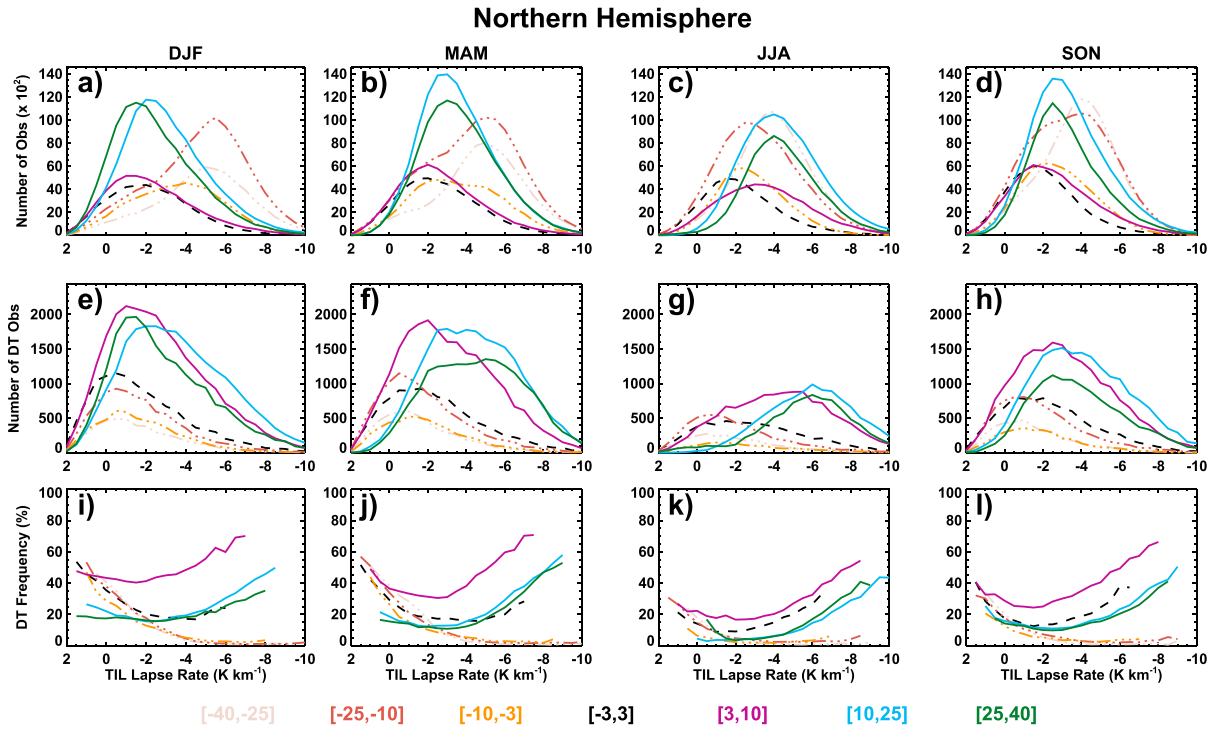

Figure 1. Distributions of the tropopause inversion layer (TIL) for the Northern Hemisphere generated using temperature data from HIRDLS Version 6 between 2005 and 2007. In these plots all data points in the Northern Hemisphere have been utilized and placed into 0.5 K km^{-1} lapse rate bins and then into latitude bins (shown at the bottom of the plot) relative to the subtropical jet using the maximum wind method. Data poleward of the jet are represented by solid lines, immediately around the jet by dashed lines, and equatorward of the jet by dash-dotted lines. Each column represents a different season (DJF = December-January-February, MAM = March-April-May, etc.), and each row presents the original data set in a different way ((a–d) total number of profiles, (e–h) total number of profiles that contain a double tropopause (DT), and (i–l) ratio of the number of DTs to the total number of profiles available, i.e., middle row divided by top row, multiplied by 100).

4. Results

4.1. Double Tropopause-Tropopause Inversion Layer Distributions

Figures 1 and 2 show distributions of the TIL strength above the primary tropopause observed in the HIRDLS data set and separated by season for vertical profiles in the Northern and Southern Hemisphere, respectively. In addition to showing distributions of the TIL strength for all vertical profiles (Figures 1a–1d and 2a–2d), these figures also show distributions of TIL strength for profiles that contain a double tropopause (DT) (Figures 1e–1h and 2e–2h) and the fraction of DT profiles, i.e., DT frequency, as a function of TIL strength (Figures 1i–1l and 2i–2l). The data are organized by latitude relative to the jet stream as discussed in section 3.3. Additionally, for clarification, the values within each TIL bin are plotted such that they are associated with the beginning of the bin, e.g., the data point associated with the [1.0, 0.5] bin can be found at x =1.0.

In Figures 1a–1d and 2a–2d the seasonal cycle of the TIL, as established by *Randel et al.* [2007b] and *Grise et al.* [2010], is evident in both the tropics (dash-dotted lines) and extratropics (solid lines) of both hemispheres. In the tropics the peak of each TIL distribution shows that the TIL is stronger, i.e., has a more negative lapse rate, in the winter and weaker in the summer. In the extratropics the TIL is stronger in the summer and weaker in the winter with the range, difference between maximum and minimum, decreasing toward the equator. Additionally, in Figures 1 and 2 the range of the TIL seasonal cycle in both the tropics and extratropics is larger in the Northern Hemisphere, consistent with a stronger Brewer-Dobson circulation due to enhanced planetary wave activity [*Holton et al.*, 1995; *Holton and Hakim*, 2013] and higher summer water vapor concentrations due to greater variability in lower stratospheric/tropospheric temperatures [*Randel and Wu*, 2010].

The TIL distribution of profiles containing a DT is presented in Figures 1e–1h and 2e–2h. The area underneath the lines in these figures represents the density of DT within each latitude band, which highlight

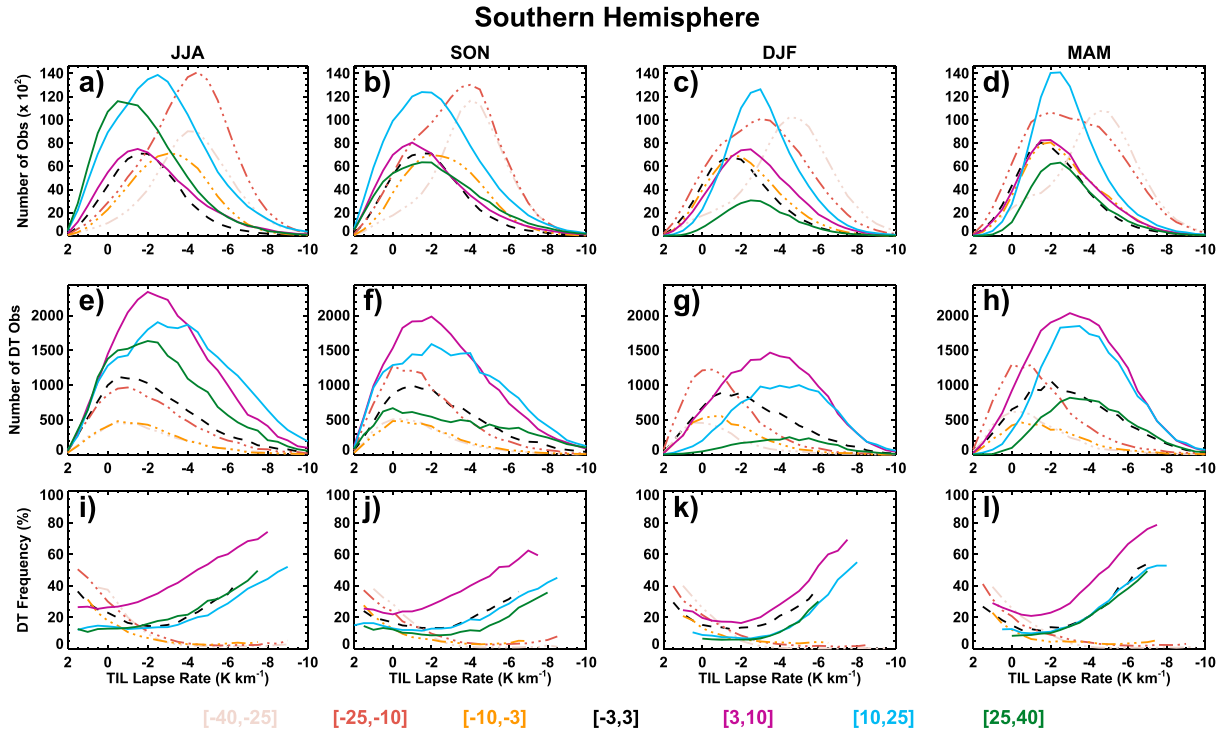

Figure 2. Same as Figure 1 but for the Southern Hemisphere. Notice that here, the left most column starts with JJA instead of DJF since JJA is the winter season in the Southern Hemisphere, thus making visual comparisons between the two hemispheres more direct.

that the highest data density occurs within the 3–10°N latitude band (this is also evident in Figures 1i–1l and 2i–2l), agreeing with previous studies [e.g., *Peevey et al.*, 2012]. For both hemispheres, the tropical TIL distributions are broad and the peak amplitudes vary little in magnitude or from season to season. In the extratropics, the maximum value of each distribution, i.e., the number of DTs, is greater in the winter than the summer, consistent with the general seasonal cycle of the DT [e.g., *Randel et al.*, 2007a; *Schmidt et al.*, 2006; *Peevey et al.*, 2012]. Additionally, the peaks of the extratropical TIL distributions have a seasonal cycle that shifts from a weaker TIL in the winter to a stronger TIL in the summer, thus following the extratropical patterns shown for the all profiles in Figures 1a–1d and 2a–2d. To further understand the DT-TIL relationship, the fraction of HIRDLS profiles with a DT as a function of the TIL lapse rate value is analyzed (see Figures 1i–1l and 2i–2l). To ensure that the sample within each latitude bin represents the population, only bins with at least ~500 profiles are shown. This is calculated using the standard z score or z test and assuming a two-tailed distribution, a margin of error of ±0.2%, and a confidence interval of 95%.

These plots (Figures 1i–1l and 2i–2l) show a clear difference in the relationship between the DT and the TIL in the tropics and the extratropics. Equatorward of the subtropical jet, the frequency of DTs decreases as a function of TIL strength for all seasons, falling below 10% around a TIL value of -2 K km^{-1} during the winter/spring months and a TIL value of around -1 K km^{-1} during the summer/fall months. Poleward of the subtropical jet, the DT frequency initially decreases with increasing TIL strength and then begins increasing around -2 K km^{-1} or -1 K km^{-1}, rapidly increasing around -5 K km^{-1}. The rate at which the DT frequency increases, i.e., the slope of the line, in each hemisphere is similar for all seasons. This is also the case for different regions, but with stronger slopes over storm track regions during the winter/spring (not shown), which further supports the overall conclusions of this study. Moreover, this relationship probably occurs within the first 2 km above the tropopause, as discussed in Appendix A, well below the 3 km limit discussed in section 3.2, thus validating the technique used to locate the TIL and showing that the DT-TIL relationship found here likely occurs close to the first tropopause. The seasonal cycle of DT frequency is apparent in Figures 1i–1l and 2i–2l in that all the lines move up (to higher percentages) in the winter/spring and move down in the summer/fall, consistent with previous studies [*Schmidt et al.*, 2006; *Peevey et al.*, 2012; *Manney et al.*, 2014]. Despite these opposing seasonal variations, the relationship of higher DT frequencies associated with stronger TILs persists, indicating a very robust relationship. Analysis of the geographical location

of weak (lapse rate > -2 K km^{-1}), medium (-2 K km^{-1} $\geq$ lapse rate > -5 K km^{-1}), and strong (lapse rate ≤ -5 K km^{-1}) TILs indicates that strong TILs do not preferentially form over regions with topographically induced gravity waves (not shown) but rather over storm track regions, further supporting the hypothesis for this study through spatial coincidence of DTs with regions of strong TILs.

Other methods for separating the tropics from the extratropics, outlined in section 3.3, show nearly identical results as those produced by the maximum wind method, further highlighting the robustness of the patterns presented in Figures 1 and 2.

4.2. Composites of Meteorological Parameters

An increasing DT frequency with increasing TIL strength within the extratropical jet-relative latitude bands suggests that the DT-TIL relationship found by *Wang and Polvani* [2011] using model simulations may also be present in the real atmosphere since there is a robust linear relationship between these two thermal structures. In this and the following sections, only results from DT cases in the Northern Hemisphere Pacific Ocean Basin are presented. Results are limited to this region since the climatological DT frequency is high and it is a predominate storm track region [e.g., *Holton et al.*, 1995; *Peevey et al.*, 2012], but results from other storm track regions are similar. To further understand why the DT occurrence frequency increases with increasing TIL strength poleward of the subtropical jet, we examine composite mean zonal cross sections of additional meteorological fields in the summer and winter seasons of each hemisphere from ERA-Interim as shown in Figures 3 and 4.

These figures are generated using the ERA-Interim 37 level data set and show how parameters associated with a DT profile change as the TIL increases in strength. We separate the Pacific ocean basin into two different regions, the eastern Pacific Ocean between 210° and 240° longitude (Figure 3) and the western Pacific Ocean between 120° and 150° longitude (Figure 4). To generate the figures shown, the data are first vertically scaled (see section 3.4), then placed into 1 km altitude bins and 3° latitude bins and averaged. The columns of each figure represent a different TIL lapse rate range ([2,−2], [−2, −5], and [−5, −10], all in units of K km^{-1}). These specific values are chosen to represent the three different regimes discussed in the previous section: (1) DT frequency decreasing with an increasing TIL strength, (2) DT frequency transitioning from decreasing to increasing with an increasing TIL strength, and (3) DT frequency increases rapidly with an increasing TIL strength. The results presented here have been found to be insensitive to the exact ranges chosen. Moreover, results are found to be nearly identical, with the majority of the differences occurring at and above the second tropopause during the winter (a season of high variability for the second tropopause), regardless of whether the vertical scaling within the DT structure is exponential instead of linear or there is no vertical scaling at all (not shown).

Figures 3 and 4 show temperature (K), vertical motion with the seasonal background atmosphere removed (Pa s^{-1}), meridional wind (m s^{-1}), and relative vorticity (10^{-4} s^{-1}). Note that only the vertical motion field has the background atmosphere removed, and all other fields are left in their original form. The vertical motion in ERA-Interim is calculated using the continuity equation in hybrid vertical coordinates [e.g., *Saarinen*, 2004]. In general, during DJF over the eastern Pacific Ocean (Figures 3a–3c) there is descending motion relative to the background atmosphere when the TIL is weak (Figures 3a and 3d), which then switches to ascending motion for higher TIL strengths (Figures 3b, 3c, 3e, and 3f). In addition, the relative vorticity throughout the troposphere is cyclonic with the strongest meridional wind located poleward of 40°N. As the strength of the TIL increases (moving from left to right in Figures 3a–3c), a temperature inversion begins to develop at an altitude of approximately 10 km, directly above a region of increased upward vertical motion. This region of increasing upward motion coincides with increases in the meridional wind speed and a change in relative vorticity from cyclonic to anticyclonic. A similar pattern also occurs in the summer over the eastern Pacific Ocean (Figures 3d–3f), but with a reduction in the magnitude of the upward vertical motion and with the relative vorticity becoming only weakly anticyclonic due to the overall weaker atmospheric circulations observed during this season [e.g., *Holton and Hakim*, 2013]. This structure is also shifted poleward during summer, in line with the seasonal cycle of the subtropical jet [e.g., *Schiemann et al.*, 2009; *Manney et al.*, 2014; *Holton and Hakim*, 2013]. Because of this movement and because there are very few DTs in the summer, some of the plots have no data at lower latitudes and/or high altitudes. In rare cases no data is available at high latitudes and altitudes (see Figure 4) because of the vertical resolution of the ERA-Interim 37 level data set at higher altitudes.

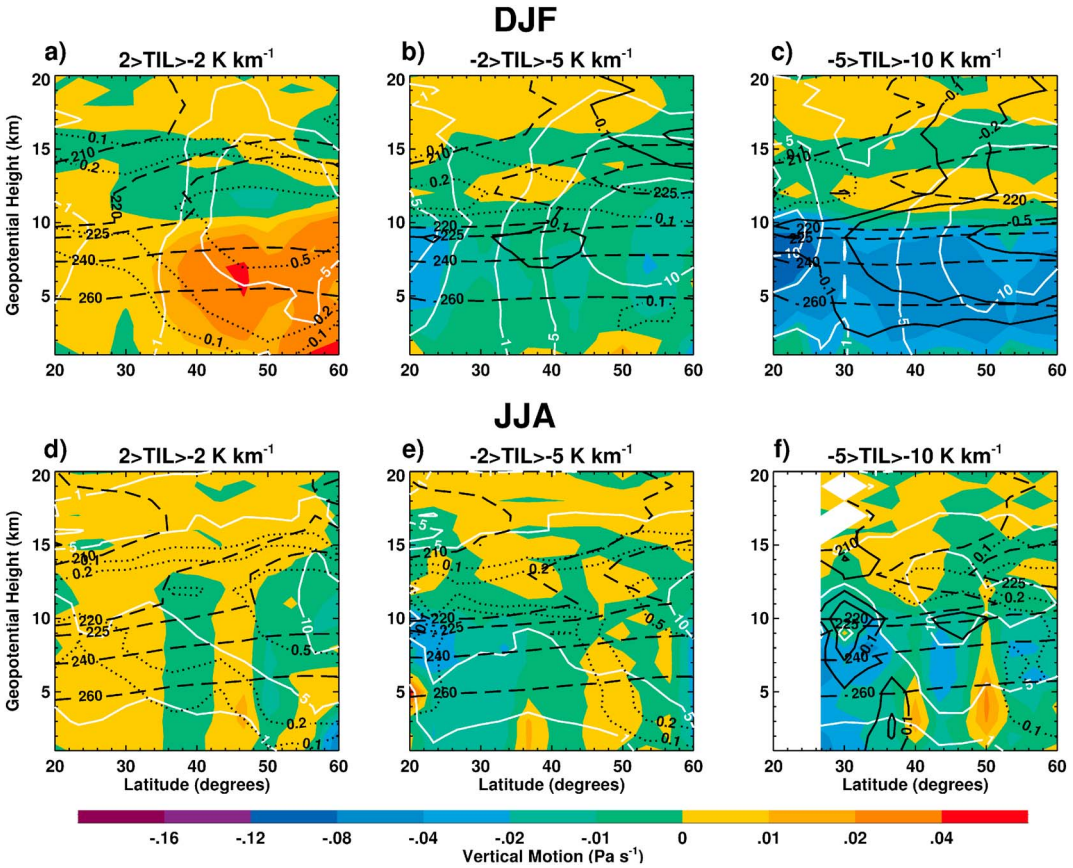

Figure 3. Zonal composites of ERA-Interim data from 2005 to 2010 for profiles that contain a DT for (a–c) DJF and (d–f) JJA. Composites are in the Northern Hemisphere and over the eastern Pacific Ocean between 210° and 240° longitude. These plots are generated by first scaling each profile vertically, as described in the text, and then placing them in altitude-latitude bins and averaging them zonally. Three different TIL strengths are shown in units of K km^{-1}: (Figures 3a and 3d) weak TIL, (Figures 3b and 3e) medium TIL, and (Figures 3c and 3f) strong TIL. Filled contours represent vertical motion, minus the background atmosphere, with positive indicating descending motion (Pa s^{-1}); black dashed lines show temperatures of 210, 220, 225, 240, and 260 K, black dotted (solid) lines show positive (negative) relative vorticity of ±0.5, ±0.2, ±0.1 × 10^{-4} s^{-1}, and white solid lines show meridional winds of 1, 5, and 10 m s^{-1}.

In the western Pacific Ocean (Figure 4) the picture is very similar to that of the eastern Pacific Ocean. In Figures 4a–4c, as the TIL increases in strength, so does the upward vertical motion and the meridional wind. The relative vorticity also switches from cyclonic to anticyclonic. A similar pattern occurs in the summer (Figures 4d–4f) but with reduced intensity. The primary difference between these two regions is the background atmosphere. The western part of the Pacific Ocean is associated with convergence aloft and descending motion since it is a jet entrance region [*Wang*, 2002; *Holton and Hakim*, 2013]. Conversely, in the eastern Pacific Ocean there is divergence aloft and ascending motion because it is a jet exit region [*Wang*, 2002; *Holton and Hakim*, 2013]. However, regardless of these differences, Figures 3 and 4 both show a tendency for downward motion relative to the background atmosphere for a weak TIL and upward motion for a strong TIL.

The relationship between the meridional wind, upward motion, and the sharpness of the tropopause presented in this section is not unexpected, because *Wirth* [2003] showed, using an idealized model, that stability just above the thermal tropopause was enhanced for anticyclonic circulations in comparison to the background atmosphere. However, the relationship between the TIL and the DT has not been identified previously in observations. Additionally, the relationship between the DT, the TIL, and the background atmosphere is interesting since strong upper tropospheric anticyclonic circulations rarely coincide with profiles that contain a DT [e.g., *Randel et al.*, 2007a]. One location within a developing baroclinic system that does have anticyclonic flow accompanied by increasing meridional wind and increasing upward motion, and is physically near the area of DT formation, is the region of the warm conveyor belt (WCB). The WCB is a

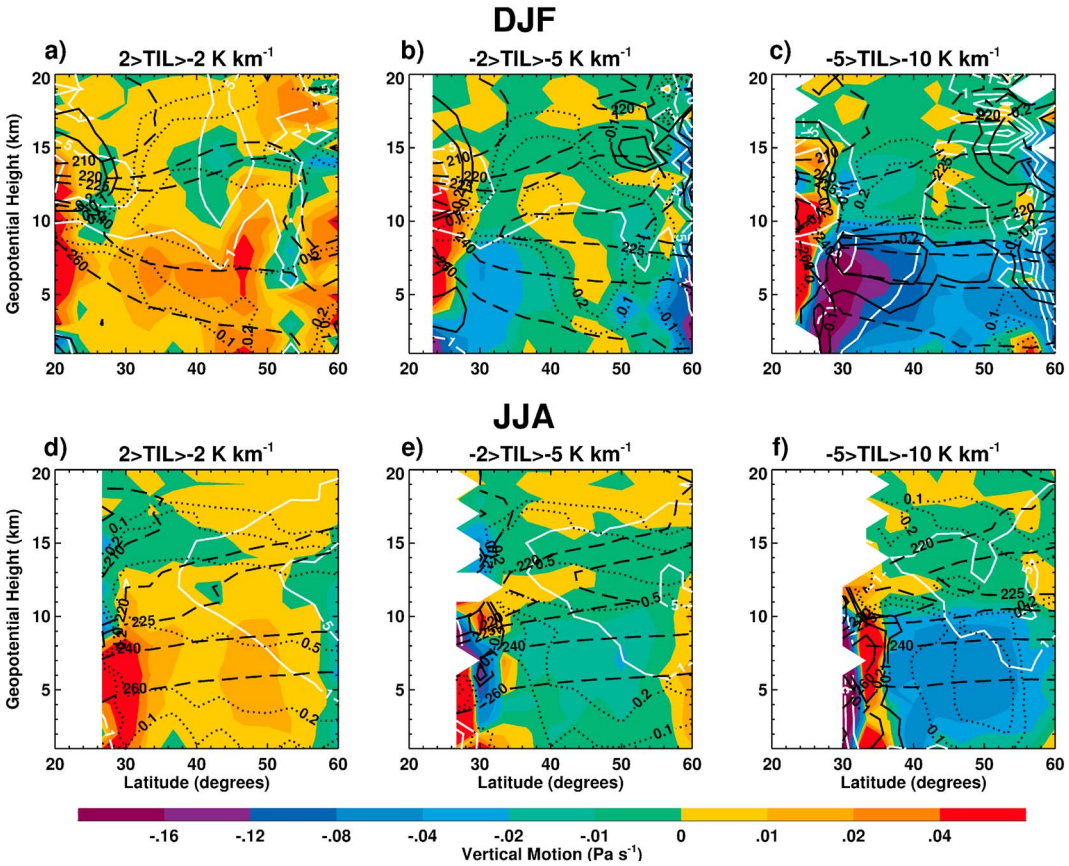

Figure 4. Same as Figure 3 but for the western Pacific Ocean between 120° and 150° longitude.

stream of poleward moving moist air that originates in the warm sector found on the anticyclonic side of the subtropical jet and can ascend to the level of the prevailing zonal winds, has its highest frequency of occurrence during the Northern Hemisphere winter over the Pacific and Atlantic oceans, and is one of the three airstreams of an extratropical cyclone [e.g., *Bjerknes*, 1910; *Harrold*, 1973; *Carlson*, 1980; *Shapiro and Grønås*, 1999; *Eckhardt et al.*, 2004; *Schemm et al.*, 2013]. Therefore, considering the above evidence, it is reasonable to infer that the WCB is the mechanism responsible for the relationship between the TIL and the DT found by *Wang and Polvani* [2011]. To further support this hypothesis, the development of a midlatitude baroclinic system is studied over a 4 day period using ERA-Interim data and presented in the next section.

4.3. Case Study

In this section we show a case study analysis of the growth and decay of a baroclinic system as it moves east across the Pacific Ocean over a 4 day period (14–17 January 2006). The ERA-Interim 60 model level data set is used to generate these plots because of its high vertical resolution (and other reasons given in section 2.3), thus helping to ensure that the full structure of the DT feature can be seen, which assists in verifying the results previously presented.

Figures 5 and 6 show the horizontal and vertical structure (along a longitude line) of a synoptic-scale storm in the Northern Hemisphere. Additionally, as the storm progresses, the vertical structure is examined a little further downstream of the surface low since the WCB is expected to be pushed eastward as the cold front catches up with the warm front. On 14 January 2006 a surface low is in its incipient stage off the coast of Japan, approximately 135° longitude (see Figure 5a). The geopotential height of the 500 hPa surface shows an associated upper level low to the west of the surface low, i.e., there is a westward tilt with height, indicating that this is a baroclinic system. Potential vorticity on the 320 K potential temperature surface is also represented using filled contours to illustrate the dynamical perspective of the system's development. The 320 K surface is chosen since the WCB, one of the air streams of a baroclinic disturbance, is usually found on lower potential temperature surfaces [e.g., *Madonna*, 2013]. Additionally, on 14 January 2006, the

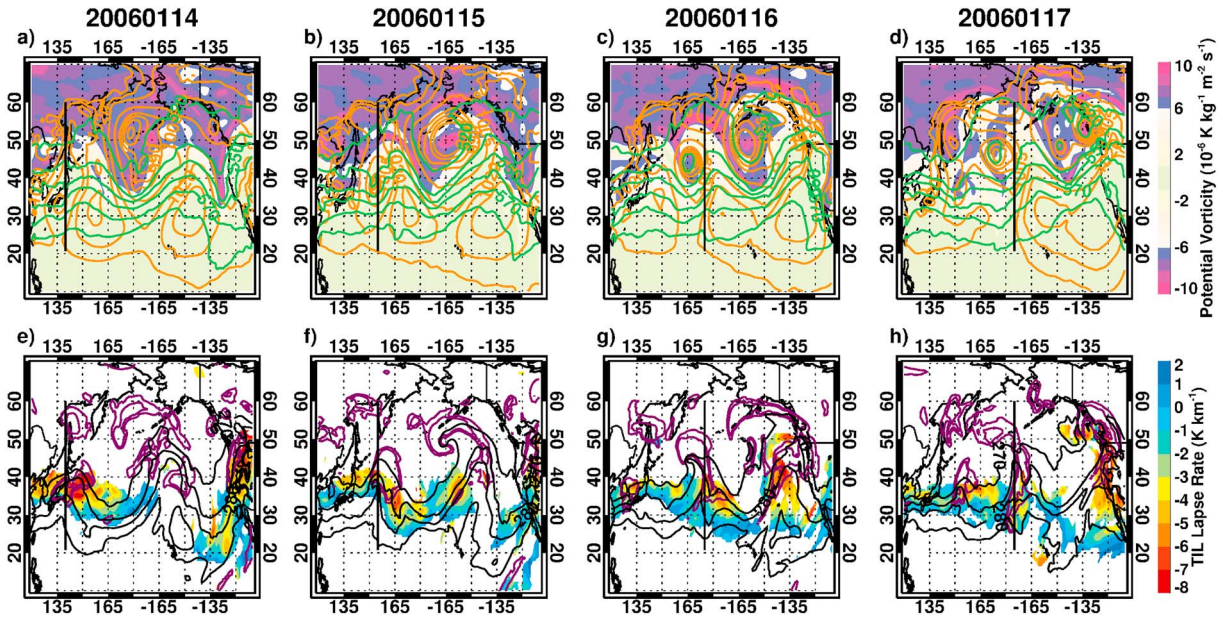

Figure 5. Horizontal view of the life cycle of a developing cyclone/baroclinic disturbance over the western Pacific Ocean from 14 to 17 January 2006. (a–d) The PV perspective of the disturbance with filled contours representing the potential vorticity on the 320 K potential temperature surface. Overlying this is surface pressure (orange lines at 980, 985, 990, 995, 1005, 1015, 1020, and 1025 hPa) and geopotential heights on the 500 hPa pressure surface (dark green lines at 520, 540, 550, 560, 570, and 580 $\times$ 10^1 m). (e–h) The thermal perspective of the disturbance. Here filled contours show the lapse rate of the TIL for DT profiles, black lines the temperature on the 840 hPa pressure surface (270, 275, 280, and 285 K), and purple lines the column cloud fraction (40 and 60%). The black line oriented north-south in all plots indicates the location of the vertical plots shown in Figure 6.

location of the WCB is evident east of the surface low, as indicated by the development of a TROWAL (Trough of Warm Air Aloft = a narrow band of warm and moist air that wraps around a cyclone) through temperature advection (Figure 5e). The development of a TROWAL also suggests that the maximum Eady growth rate is increasing since the local meridional temperature gradient is increasing near the surface, which is proportional to vertical shear, a component of the Eady growth rate formula (see *Hendricks et al.* [2014], equation (1)), through the thermal wind equation. These horizontal plots show the development of a baroclinic system as it first forms on 14 January 2006, strengthens on 15 January 2006 due to the upper level divergence, appears to reach its maximum strength on 16 January 2006, and then begins to dissipate once the lower and upper level lows are no longer tilted in the vertical, i.e., stacked, on 17 January 2006.

During the growth and decay of the baroclinic system the vertical structure downstream of the center of the surface low is also examined (see Figure 6). On 14 January 2006, the vertical cross sections show that air is ascending at 30°N and moving poleward within a region that is a mixture of anticyclonic and cyclonic motion below the tropopause (see Figure 6a). Air is descending poleward and equatorward of this point and therefore does not yet clearly show the classic characteristics of the WCB as discussed previously. However, examination of the vertical profiles directly over the surface low (not shown) does show air ascending in the warm sector and then descending poleward of that location, a motion that is indicative of the WCB.

Over the next 2 days, as the baroclinic disturbance strengthens, the horizontal structure shows a deepening TROWAL and the development of a clearly defined cloud pattern (Figures 5f and 5g), which helps to identify the location of the WCB within the developing disturbance [*Browning*, 1990]. Moreover, the PV perspective of the structure indicates that the system is broadening and wrapping up cyclonically, characteristics of a LC2 baroclinic disturbance (Figures 5b and 5c). At the same time the upward vertical motion within the WCB is increasing, and the relative vorticity is becoming more anticyclonic (Figures 6b, 6c, 6f, and 6g). Changes in the vertical motion and relative vorticity are most prominent on 16 January 2006 at ~30°N (Figures 6c and 6g), when the baroclinic disturbance has matured. On this day the meridional extent of the TIL and the DT downstream of the surface low has increased significantly, moving equatorward via an extension of the extratropical tropopause. The horizontal extent of this structure is evident in Figure 5g. This figure also further highlights the relationship between the DT, the TIL, and the WCB since the increase in the meridional

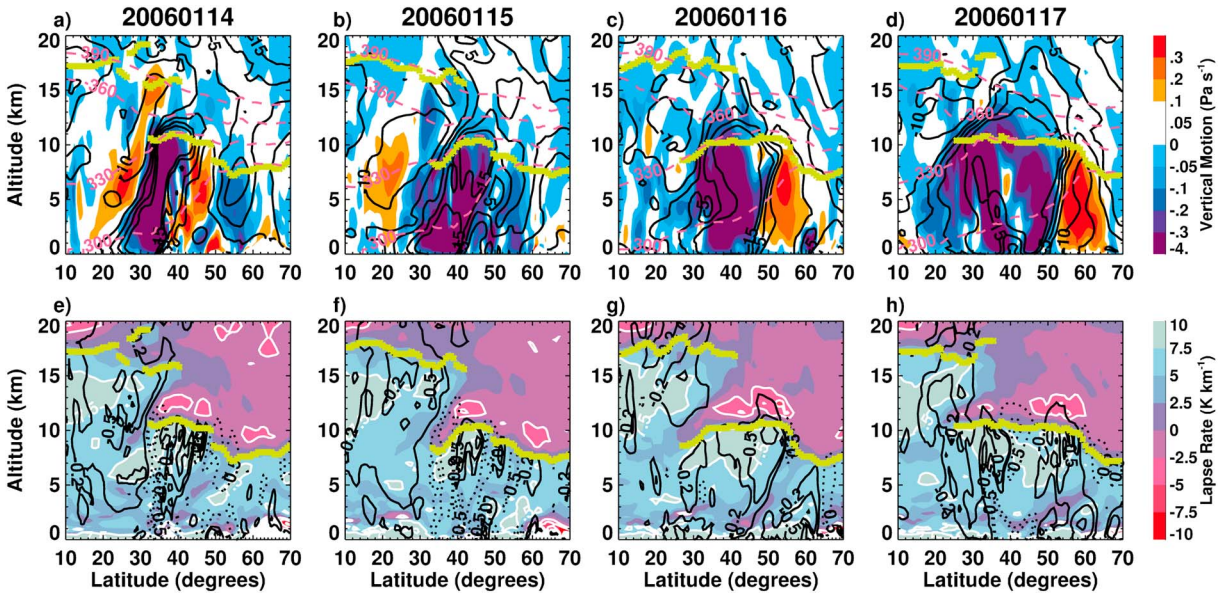

Figure 6. Same dates as Figure 5 but showing the vertical structure downstream of the surface low pressure system, as indicated by the black line in Figure 5. (a–d) The filled contours represent vertical motion (blue = upward motion) and are overlaid by potential temperature (pink dashed lines at 300, 330, 360, and 390 K), meridional wind (black solid lines at −10, 0, 5, 10, and 15 m s^{-1}), and the location of the first and second tropopause (green asterisks). (e–h) The following fields are plotted: lapse rate (filled contours, white contour lines at −10, −5, −2.5, and 7.5 K km^{-1}), relative vorticity (dotted lines at 0.5 and 1.0 $\times 10^{-4}$ s^{-1}; solid lines at −0.2, −0.5, −1.0 10^{-4} s^{-1}), and the location of the first and second tropopause (green asterisks).

extent of the DT structure spatially coincides with the location of large cloud fractions, a strong TIL and a deep or well-developed TROWAL.

On 17 January 2006 the disturbance is starting to weaken, as evident in the decrease in the north-south pressure and potential vorticity gradients. At the same time the strength of the TIL, the meridional extent of the DT, and the TROWAL have all decreased significantly. The cyclone remains stacked into the next day, after which it dissipates (not shown).

5. Discussion

The results presented above show a robust global relationship between the DT and the TIL where the DT frequency increases (decreases) in the extratropics (tropics) as the TIL increases in strength. Zonal composites and a case study suggest that the warm conveyor belt (WCB) may be the mechanism responsible for this relationship in the extratropics. The case study specifically shows the equatorward extension of the DT above the WCB as it expands meridionally and the cyclone strengthens. This result is consistent with that found in *Wang and Polvani* [2011] and has several implications, which are presented and discussed below along with comparisons to other studies.

The seasonal cycle of the tropopause inversion layer (TIL) (Figures 1a–1d and 2a–2d) indicates that it is stronger in the winter (summer) and weaker in the summer (winter) in the tropics (extratropics), in agreement with previous work [e.g., *Birner*, 2006; *Randel et al.*, 2007b; *Grise et al.*, 2010; *Son et al.*, 2011]. Additionally, these figures show that the extratropical TIL seasonal cycle becomes weaker when moving from polar regions to the subtropical jet. This is consistent with *Son et al.* [2011], who suggested that the midlatitude variability of the Brunt Väisälä frequency is controlled by stationary waves and storm tracks on interseasonal time scales and, more importantly, could be related to the frequent occurrence of DTs in the subtropics on intraseasonal time scales. Moreover, a global spatial analysis of profiles with strong TILs (lapse rate < -5 K km^{-1}) further supports the connection between the DT and TIL since it shows that many of these profiles are located in regions of DT formation (not shown). Within a few degrees and on the cyclonic side of the subtropical jet, the TIL strength has the weakest seasonal cycle, which could be partly due to synoptic-scale eddies that mix low O_3 and high H_2O air masses that are associated with low N^2 values above the extratropical thermal tropopause [*Kunz et al.*, 2009].

In Figures 1 and 2 the peak of the extratropical TIL distributions for DT profiles is greater in the winter than in the summer. This is most likely due to seasonal changes in the strength of atmospheric circulations [*Randel et al.*, 2007a], such as cyclonic circulations associated with weather systems [*Wernli and Schwierz*, 2006], and variations in jet strength and distribution [*Manney et al.*, 2014]. In Figures 1i–1l and 2i–2l, DT frequency is shown to generally be inversely related (proportional) to the TIL in the tropics (extratropics) such that as the strength of the TIL increases the frequency of the DT decreases (increases). In the tropics this suggests that regions of strong TIL, currently thought to be a product of deep convection that reaches the tropopause [*Grise et al.*, 2010; *Son et al.*, 2011; *Biondi et al.*, 2012], are coincident with single tropopause profiles rather than double tropopause profiles. During JJA in the Northern Hemisphere the subtropical jet moves poleward, and therefore, some of the results shown in Figure 1 for this season could result from TIL formation due to the increase of water vapor during the polar summer [*Randel and Wu*, 2010]. However, regardless of the formation mechanism of the TIL, its relationship to DT formation in the extratropics seems quite robust since the connection is consistent in Figures 1 and 2 regardless of the exact longitude range used (not shown).

To explore the mechanism behind the DT-TIL relationship in midlatitudes, zonal composites were generated over the Pacific Ocean using ERA-Interim profiles that contain a DT. These composites show an increase in the upward vertical motion and meridional wind along with a clear transition from positive to negative relative vorticity with increasing TIL strength. Examination of Figures 1 to 4 show that the majority of DTs coincide with weak TILs and therefore are also strongly associated with cyclonic circulations in the UTLS, in agreement with work by *Randel et al.* [2007a]. However, results from the case study presented here show that there could be a significant relationship between DTs and upper tropospheric anticyclonic circulation. Therefore, that distribution may not be an accurate representation of the relationship found here since the anticyclonic motion shown in Figures 3 and 4 occurs below the first tropopause, which is generally at pressures greater than 200 hPa during the winter-spring season in the extratropics [*Añel et al.*, 2008; *Peevey et al.*, 2012]. Even though the relationship between the TIL, vertical motion, and relative vorticity is not unexpected [*Wirth*, 2003; *Wirth and Szabo*, 2007], the relationship between these meteorological variables and the DT is interesting since the DT rarely form above strong upper tropospheric anticyclonic circulations [*Randel et al.*, 2007a]. Therefore, the relationship between the DT and tropospheric dynamics discussed here could be stronger and more complex than previously thought.

The relationship between the upward vertical motion, anticyclonic circulation, and the meridional wind in midlatitudes suggests that a mechanism by which the extratropical DT can form in relation with the TIL is the WCB. *Randel et al.* [2007a] interpreted reduced ozone levels within the DT as an indication that it is a region of enhanced transport and suggested multiple mechanisms for this transport, which included the thermally direct circulation. This study shows that such a relationship may exist (see Figures 5 and 6) since the large-scale upper level flow does play a role in supporting the development of lower level baroclinic instabilities [*Holton and Hakim*, 2013]. During this event the meridional extent of the DT structure increases as the WCB and consequently the TIL strengthen. Though this mechanism is shown only for the Northern Hemisphere, similar results should be found in the Southern Hemisphere since the same DT-TIL relationship is found there (see Figures 2i–2l) and WCBs are frequent in the Southern Hemisphere during the winter [*Eckhardt et al.*, 2004]. The results from the case study are in line with the theoretical results of *Wang and Polvani* [2011] except that the DT formed in *Wang and Polvani* [2011] had a slightly larger meridional extent than that shown on 16 January 2006 (see Figure 6). This could be because *Wang and Polvani* [2011] used a dry model since the WCB is a moist airstream that produces negative PV anomalies above the level of maximum diabatic heating, which enhances upper level ridges that have been shown to lead to more rapid cyclogenesis and downstream Rossby wave breaking [*Wernli and Davies*, 1997; *Massacand et al.*, 2001; *Joose and Wernli*, 2012; *Schemm et al.*, 2013]. Additionally, only one case study is analyzed in this work and the meridional extent is likely to vary between cases. More research is required to generate a climatology of the observed characteristics and relationship of the DT to the WCB.

Examination of Figures 1, 5, and 6 has revealed an interesting relationship between the TIL and DT formation. This analysis suggests a potential role for additional aspects of tropospheric dynamics in DT formation and highlights the complexity of the processes that couple the troposphere to the stratosphere. This research may also help explain the current conflicting evidence for the origin of air within the DT [*Pan et al.*, 2009; *Wang and Polvani*, 2011; *Añel et al.*, 2012]. During the first few days of growth of the baroclinic disturbance, Figures 5 and 6 show that the upper/second tropopause only extends poleward about ~5° where

the lower/first tropopause extends ~15° equatorward. This could imply that on average, the movement of air within the DT structure is from high latitudes to low latitudes, as shown by *Wang and Polvani* [2011]. This is also in line with the tendency of LC2 baroclinic disturbances to have significantly larger transport from the stratosphere into the troposphere relative to LC1 disturbances [*Polvani and Esler*, 2007]. As the system shown in this study develops, it becomes stacked and dissipates and does not appear to result in a Rossby wave breaking event. However, if it did, then the average air movement could switch and instead move from low latitudes to high latitudes, as shown by *Pan et al.* [2009]. Therefore, the overall movement of air and the potential impact of the DT on the composition of the UTLS and its association with STE may depend upon the state of development, or other case-to-case variations, of the system. Further work, such as performing trajectory analyses of a variety of baroclinic systems during each stage of their development, would be needed to confirm this hypothesis. Moreover, an analysis of this relationship beyond individual events would also be needed to fully establish the robustness of the relationship presented here. Such a study could isolate baroclinic systems using a well-known Baroclinic Activity Index (e.g., Eady growth rate) and WCBs using techniques presented in *Schemm et al.* [2013], for example, and then examine their global occurrence in relation to DT frequency.

This study shows a relationship between the DT and the TIL within WCBs, an unexpected relationship since these atmospheric phenomena have opposing seasonal characteristics and formation mechanisms [*Wang and Polvani*, 2011]. This demonstrates that the DT is more complicated than prior poleward transport studies might suggest and requires even further study to understand its relationship with the many STE and non-STE processes present in the UTLS.

6. Conclusions

Knowledge of the UTLS is critical to understanding Earth's changing climate because of the radiative sensitivity of this region of the atmosphere [e.g., *Gettelman et al.*, 2011]. Within this region of the atmosphere lies the DT, the focus of this study. Characteristics of the DT include its association with poleward Rossby wave breaking [e.g., *Pan et al.*, 2009; *Homeyer et al.*, 2011] and its tendency to occur during the Northern Hemisphere winter/spring over the Pacific and Atlantic oceans, both storm track regions [e.g., *Añel et al.*, 2008; *Castanheira and Gimeno*, 2011; *Peevey et al.*, 2012]. This geographical relationship between DTs and storm track regions prompted *Wang and Polvani* [2011] to examine the formation of the DT during the idealized LC1/2 baroclinic life cycles, which showed a direct relationship between DT formation and TIL strength. Largely motivated by these results, we examined the DT-TIL relationship using satellite observations from HIRDLS and reanalyses from ERA-Interim. Similar to the modeling results in *Wang and Polvani* [2011], we found that as the stability within the TIL increased, so did the relative frequency of DTs. Therefore, we suggest that the warm conveyor belt (WCB) is the mechanism responsible for this relationship.

Understanding the DT-TIL relationship is important because of its location in the UTLS, as stated above, and because even though the DT has been well documented, the DT-TIL relationship is not known. Additionally, the connection to the WCB is interesting because it is a significant atmospheric structure that has been shown to occur within extratropical cyclones about 60% (35%) of the time during the Northern (Southern) Hemisphere winter [*Eckhardt et al.*, 2004]. The results presented in this study could thus have important implications for the composition of the UTLS, since the WCB is one of the three air streams within an extratropical cyclone that is responsible for most of the meridional energy transport (latent and sensible) and rapid transport from the boundary layer into the UTLS [e.g., *Stohl et al.*, 2001, 2003; *Eckhardt et al.*, 2004]. Pollutants such as ozone, once deposited into the UTLS, then have the potential to enter the lower stratosphere and consequently change the Earth's radiative balance and climate [e.g., *Gettelman et al.*, 2011]. Additionally, previous studies have suggested that synoptic-scale activity is the reason for the increased DT activity over storm track regions [e.g., *Añel et al.*, 2012]. This study has verified this possibility and has shown examples supporting the relationship. The work presented here also offers some insight into differing results from previous studies of the origin of air within the DT, showing that the origins of that air likely depend upon the dynamical development of the system associated with each DT occurrence. This complexity should be considered in future investigations of the DT.

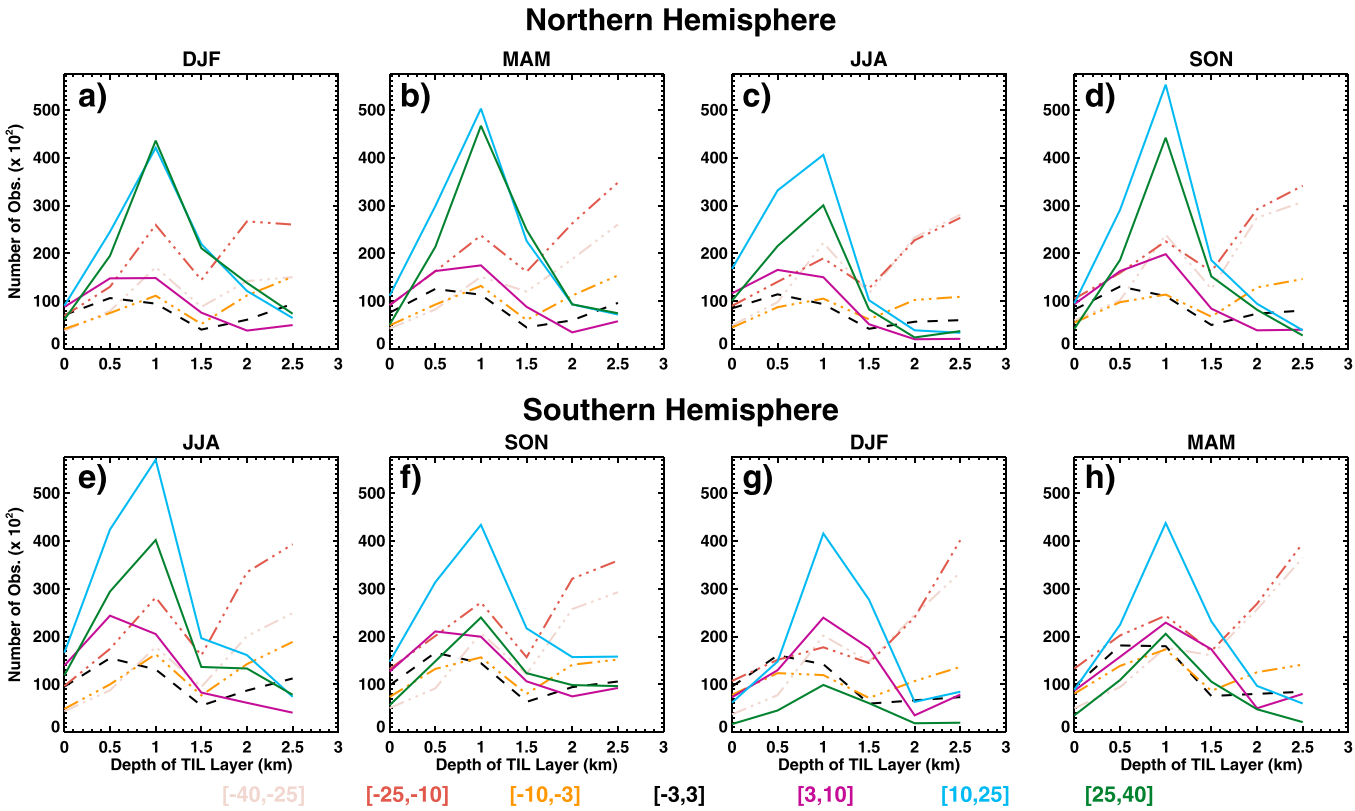

Figure A1. Distributions of the depth (altitude of tropopause inversion layer (TIL)-altitude of first tropopause) of the TIL for the (a–d) Northern Hemisphere and (e–h) Southern Hemisphere generated using temperature data from HIRDLS Version 6 between 2005 and 2007. In these plots all data points in the Northern Hemisphere have been utilized and placed into 0.5 km altitude bins and then placed into latitude bins (shown at the bottom of the plot) relative to the subtropical jet using the maximum wind method. Data poleward of the jet are represented by solid lines, immediately around the jet by dashed lines, and equatorward of the jet by dash-dotted lines. Each column represents the different seasons (DJF = December-January-February, MAM = March-April-May, etc.) of each hemisphere, e.g., first column shows the winter season, the second column the spring season, etc.

The primary results from this study are the following:

1. Zonal distributions of the TIL, generated using HIRDLS data, highlight the seasonal cycle of the TIL (stronger in the winter/summer in the tropics/extratropics) as a function of latitude from the subtropical jet, in agreement with previous studies [e.g., *Randel et al.*, 2007b; *Grise et al.*, 2010].
2. DT frequency distributions in relation to TIL strength show that the frequency of DTs decreases in the tropics as the strength (or stability) of the TIL increases. In the extratropics DT frequency initially decreases with increasing TIL strength until about -2 K km^{-1}. For stronger TILs the frequency of DTs increases, at first slowly and then more rapidly above -5 K km^{-1}. This relationship between the DT and the TIL is found in all seasons and both hemispheres and does not depend on the technique used to define the tropics and extratropics.
3. Most of the variability associated with the seasonal cycle of the tropical TIL appears to be associated with profiles containing only one tropopause, that is, having no DT.
4. Zonal composites of DT profiles over the Pacific Ocean reveal that as the TIL becomes stronger, the relative vorticity switches from cyclonic to anticyclonic and both the upward motion and meridional wind increase. The above results suggest the WCB as a mechanism responsible for the observed DT-TIL relationship in the extratropics; this was confirmed in a case study.
5. DT formation during the development of a baroclinic disturbance and the associated WCB is the result of an equatorward expansion of the lower extratropical tropopause rather than the poleward expansion of the tropical tropopause, as observed in previous studies of Rossby wave breaking.

Appendix A: Vertical Location of the TIL

To verify the technique used to locate the TIL in this study, Figure A1 is generated using the same binning technique used for Figures 1 and 2, except that instead of binning by lapse rate, the data are binned by altitude. The presentation of the data is the same also, e.g., the data point at $x = 0.5$ represents the number of TILs located within the 0.5–1.0 km altitude bin. This figure shows the altitude of the maximum stability (i.e., the TIL) relative to the first tropopause for all profiles. In this figure the extratropical TIL is found within the first 0.5 to 1.5 km above the tropopause the majority of the time, highlighting the accuracy of the technique used to find the TIL and suggesting that most of the interesting features found in Figures 1 and 2 are a product of changes in the UTLS directly above the first tropopause. Some TILs are also found above 2 km, which is likely the result of either the stability within the TIL layer peaking at a higher altitude or the stability upon entering the stratosphere being larger than that of the TIL at lower levels. However, regardless of the source, this feature is not a strong nor consistent and thus is not a concern. In the tropics most of the panels show two peaks, which agrees with previous studies showing the location of the tropical TIL at 1 and 3 km above the first tropopause [*Grise et al.*, 2010]. When considering only profiles that contain a DT, these structures are also found, but with two differences: in the tropics the second peak between 2.5 and 3 km is no longer present, and in the extratropics the amplitude of the [3, 10] latitude bin line is greater than the other lines rather than less than (not shown).

Acknowledgments

This work is supported in part by NASA's AURA satellite program under contract NAS5-97046. Assistance related to facilities and technology is also provided by the National Center for Atmospheric Research in Boulder, CO, and partly by Forschungzentrum Jülich in Jülich, Germany. Thanks to many colleagues at both of these facilities for stimulating conversations and constructive criticisms. Additional thanks to the HIRDLS team for their efforts to continually improve the HIRDLS data set and William H. Daffer at the Jet Propulsion Laboratory (JPL) for providing jet core locations in relation to the HIRDLS data set. Finally, we would like to give special thanks to Anne Kunz, Rolf Müller, and Paul Konopka for the helpful discussions and insights. HIRDLS, GEOS5, and ERA-Interim data can be downloaded from the following websites: http://disc.sci.gsfc.nasa.gov/Aura/data-holdings/HIRDLS, http://gmao.gsfc.nasa.gov/products/, and http://apps.ecmwf.int/datasets/data/interim_full_daily/?levtype=ml, respectively.

References

Añel, J. A., J. C. Antuña, L. de la Torre, J. M. Castanheira, and L. Gimeno (2008), Climatological features of global multiple tropopause events, *J. Geophys. Res.*, *113*, D00B08, doi:10.1029/2007JD009697.

Añel, J. A., L. de la Torre, and L. Gimeno (2012), On the origin of air between multiple tropopauses at midlatitudes, *Sci. World J.*, 191028, doi:10.1100/2012/191028.

Barnes, E. A., and D. L. Hartmann (2012), Detection of Rossby wave breaking and its response to shifts of the midlatitude jet with climate change, *J. Geophys. Res.*, *117*, D09117, doi:10.1029/2012JD017469.

Berrisford, P., D. P. Dee, P. Poli, R. Brugge, K. Fielding, M. Fuentes, P. Kållberg, S. Kobayashi, S. M. Uppala, and A. Simmons (2011), *'The ERA-Interim Archive'*, 2nd ed., ERA Report Series, ECMWF, Reading, U. K.

Biondi, R., W. J. Randel, S.-P. Ho, T. Neubert, and S. Syndergaard (2012), Thermal structure of intense convective clouds derived from GPS radio occultations, *Atmos. Chem. Phys.*, *12*, 5309–5318, doi:10.5194/acp-12-5309-2012.

Birner, T. (2006), Fine-scale structure of the extratropical tropopause region, *J. Geophys. Res.*, *111*, D04104, doi:10.1029/2005JD006301.

Birner, T. (2010), Residual circulation and tropopause structure, *J. Atmos. Sci.*, *67*, 2582–2600.

Birner, T., A. Dörnbrack, and U. Schumann (2002), How sharp is the tropopause at midlatitudes?, *Geophys. Res. Lett.*, *29*(14), 45-1–45-4, doi:10.1029/2002GL015142.

Bjerknes, J., and E. Palmen (1937), *Investigation of Selected European Cyclones by Means of Serial Ascents*, Geofis. Publ., vol. 12, Am. Meteorol. Soc., Boston, Mass.

Bjerknes, V. (1910), Synoptical representation of atmospheric motions, *Q. J. R. Meteorol. Soc.*, *36*, 267–286.

Browning, K. A. (1990), Organization of clouds and precipitation in extratropical cyclones, in *Extratropical Cyclones; The Erik Palmen Memorial Volume*, edited by C. W. Hewson and E. O. Holopainen, chap. 8, pp. 129–153, Am. Meteorol. Soc., Boston, Mass.

Carlson, T. N. (1980), Airflow through midlatitude cyclones and the comma cloud pattern, *Mon. Weather Rev.*, *108*, 1498–1509.

Castanheira, J. M., and L. Gimeno (2011), Association of double tropopause events with baroclinic waves, *J. Geophys. Res.*, *116*, D19113, doi:10.1029/2011JD016163.

Castanheira, J. M., J. A. Añel, C. A. F. Marques, J. C. Antuña, M. L. R. Liberato, L. de la Torre, and L. Gimeno (2009), Increase of upper troposphere/lower stratosphere baroclinicity during the second half of the 20th century, *Atmos. Chem. Phys.*, *9*, 9143–9153.

Castanheira, J. M., T. R. Peevey, C. A. F. Marques, and M. A. Olsen (2012), Relationships between Brewer-Dobson circulation, double tropopauses, ozone and stratospheric water vapour, Atmos, *Chem. Phys.*, *12*, 10,195–10,208.

Chang, E. K. M., S. Lee, and K. L. Swanson (2002), Storm track dynamics, *J. Clim.*, 2163–2183.

Chung, E.-S., B. Soden, B. Sohn, and J. Schmetz (2013), An assessment of the diurnal variation of upper tropospheric humidity in reanalysis datasets, *J. Geophys. Res. Atmos.*, *118*, 3425–3430, doi:10.1002/jgrd.50345.

Danielsen, E. F. (1959), The laminar structure of the atmosphere and its relation to the concept of a tropopause, *Arch. Meteorol. Geophys. Bioklimatol. Ser. A*, *11*, 293–332.

Dee, D. P., et al. (2011), The ERA-Interim reanalysis: Configuration and performance of the data assimilation system, *Q. J. R. Meteorol. Soc.*, *137*, 553–597, doi:10.1002/qj.828.

Eckhardt, S., A. Stohl, H. Wernli, P. James, C. Forster, and N. Spichtinger (2004), A 15 year climatology of warm conveyor belts, *J. Clim.*, *17*, 218–237.

Esler, J. G., and P. H. Haynes (1999), Baroclinic wave breaking and the internal variability of the tropospheric circulation, *J. Atmos. Sci.*, *56*, 4014–4031.

Fahey, D. W., A. R. Douglass, V. Ramaswamy, and A.-M. Schmoltner (2008), How do climate change and stratospheric ozone loss interact?, in *Trends in Emissions of Ozone-Depleting Substances, Ozone Layer Recovery, and Implications for Ultraviolet Radiation Exposure*, edited by A. R. Ravishankara, M. J. Kurylo, and C. A. Ennis, 2.4 ed., pp. 111–132, Department of Commerce, NOAA's National Climatic Data Center, Asheville, North California. a Report by the U.S. Climate Change Science Program and the Subcommittee on Global Change Research.

Garcia, R., and W. Randel (2008), Acceleration of the Brewer-Dobson circulation due to increases in greenhouse gases, *J. Atmos. Sci.*, *65*, 2731–2739, doi:10.1175/2008JAS2712.1.

Gettelman, A., P. Hoor, L. L. Pan, W. J. Randel, M. I. Hegglin, and T. Birner (2011), The extratropical upper troposphere and lower stratosphere, *Rev. Geophys.*, *49*, RG3003, doi:10.1029/2011RG000355.

Gille, J. C., and L. J. Gray (2011), High Resolution Dynamics Limb Sounder Earth Observing System (EOS) data description and quality, *Tech. Rep.* [Available at http://www.eos.ucar.edu/hirdls/data/products/HIRDLS-DQD-V6-1.pdf.]

Gille, J. C., et al. (2008), The High Resolution Dynamics Limb Sounder (HIRDLS): Experiment, overview, recovery, and validation of initial temperature data, *J. Geophys. Res.*, *113*, D16S43, doi:10.1029/2007JD008824.

Grise, K. M., D. W. J. Thompson, and T. Birner (2010), A global survey of static stability in the stratosphere and upper troposphere, *J. Clim.*, *23*, 2275–2292.

Harrold, T. (1973), Mechanisms influencing distribution of precipitation within baroclinic disturbances, *Q. J. R. Meteorol. Soc.*, *99*, 232–251.

Hendricks, E., J. Doyle, S. Eckermann, Q. Jiang, and P. Reinecke (2014), What is the source of the stratospheric gravity wave belt in austral winter, *J. Atmos. Sci.*, *71*, 1583–1592, doi:10.1175/JAS-D-13-0332.1.

Hoinka, K. P. (1997), The tropopause: Discovery, definition and demarcation, *Meteorol. Z.*, *6*(6), 281–303.

Holton, J. R., and G. J. Hakim (2013), *An Introduction to Dynamic Meteorology,* 5th ed., Academic Press, London, U. K.

Holton, J. R., P. Haynes, M. E. McIntyre, A. R. Douglass, R. B. Rood, and L. Pfister (1995), Stratosphere-troposphere exchange, *Rev. Geophys.*, *33*, 403–439.

Homeyer, C. R., K. P. Bowman, and L. L. Pan (2010), Extratropical tropopause transition layer characteristics from high-resolution sounding data, *J. Geophys. Res.*, *115*, D13108, doi:10.1029/2009JD013664.

Homeyer, C. R., K. P. Bowman, L. L. Pan, E. L. Atlas, R. Gao, and T. L. Campos (2011), Dynamical and chemical characteristics of tropospheric intrusions observed during START08, *J. Geophys. Res.*, *116*, D06111, doi:10.1029/2010JD015098.

Joose, H., and H. Wernli (2012), Influence of microphysical processes on the potential vorticity development in a warm conveyor belt: A case-study with the limited-area model COSMO, *Q. J. R. Meteorol. Soc.*, *138*, 407–418, doi:10.1002/qj.934.

Khosravi, R., et al. (2009), Overview and characterization of retrievals of temperature, pressure, and atmospheric constituents from the High Resolution Dynamic Limb Sounder (HIRDLS) measurements, *J. Geophys. Res.*, *114*, D20304, doi:10.1029/2009JD011937.

Kochanski, A. (1955), Cross sections of the mean zonal flow and temperature along 80°W, *J. Meteorol.*, *12*, 95–106.

Kunz, A. (2009), Observation - and model - based study of the extratropical UT/LS, PhD thesis, Univ. of Wuppertal, Wuppertal, Germany.

Kunz, A., P. Konopka, R. Müller, L. L. Pan, C. Schiller, and F. Rohrer (2009), High static stability in the mixing layer above the extratropical tropopause, *J. Geophys. Res.*, *114*, D16305, doi:10.1029/2009JD011840.

Kunz, A., L. L. Pan, P. Konopka, D. E. Kinnison, and S. Tilmes (2011a), Chemical and dynamical discontinuity at the extratropical tropopause based on START08 and WACCM analyses, *J. Geophys. Res.*, *116*, D24302, doi:10.1029/2011JD016686.

Kunz, A., P. Konopka, R. Müller, and L. L. Pan (2011b), Dynamical tropopause based on isentropic potential vorticity gradients, *J. Geophys. Res.*, *116*, D01110, doi:10.1029/2010JD014343.

Lahoz, W. A., S. A. Buehler, and G. Legras (2007), The COST 723 Action, *Q. J. R. Meteorol. Soc.*, *133*, 99–108, doi:10.1002/qj.158.

Madonna, E. (2013), Warm conveyor belts, climatology and forecast performance, PhD thesis, Diss. ETH NO. 21315, ETH Zurich, Switzerland.

Manney, G., M. Hegglin, W. Daffer, M. Schwartz, M. Santee, and S. Pawson (2014), Climatology of Upper Tropospheric/Lower Stratospheric (UTLS) jets and tropopauses in MERRA, *J. Clim.*, *27*, 3248–3271, doi:10.1175/JCLI-D-13-00243.1.

Manney, G. L., et al. (2011), Jet characterization in the Upper Troposphere/Lower Stratosphere (UTLS): Applications to climatology and transport studies, *Atmos. Chem. Phys.*, *11*, 6115–6137.

Massacand, A. C., H. Wernli, and H. C. Davies (2001), Influence of upstream diabatic heating upon an Alpine event of heavy precipitation, *Mon. Weather Rev.*, *129*, 2822–2828.

Olsen, M. A., A. R. Douglass, M. R. Schoeberl, J. M. Rodriquez, and Y. Yoshida (2010), Interannual variability of ozone in the winter lower stratosphere and the relationship to lamina and irreversible transport, *J. Geophys. Res.*, *115*, D15305, doi:10.1029/2009JD013004.

Pan, L. L., and L. A. Munchak (2011), Relationship of cloud top to the tropopause and jet structure from CALIPSO data, *J. Geophys. Res.*, *116*, D12201, doi:10.1029/2010JD015462.

Pan, L. L., W. J. Randel, J. C. Gille, W. D. Hall, B. Nardi, S. Massie, V. Yudin, R. Khosravi, P. Konopka, and D. Tarasick (2009), Tropospheric intrusions associated with the secondary tropopause, *J. Geophys. Res.*, *112*, D10302, doi:10.1029/2008JD011374.

Peevey, T. R. (2013), Observations of the UTLS: An analysis of the double tropopause and its relationship to Rossby waves and the tropopause inversion layer, PhD thesis, Univ. of Colo., Boulder.

Peevey, T. R., J. C. Gille, C. E. Randall, and A. Kunz (2012), Investigation of double tropopause spatial and temporal global variability utilizing HIRDLS temperature observations, *J. Geophys. Res.*, *117*, D01105, doi:10.1029/2011JD016443.

Polvani, L. M., and J. G. Esler (2007), Transport and mixing of chemical air masses in idealized baroclinic life cycles, *J. Geophys. Res.*, *112*, D23102, doi:10.1029/2007JD008555.

Randel, W. J., and F. Wu (2010), The polar summer tropopause inversion layer, *J. Atmos. Sci.*, *67*, 2572–2581.

Randel, W. J., D. J. Seidel, and L. L. Pan (2007a), Observational characteristics of double tropopauses, *J. Geophys. Res.*, *112*, D07309, doi:10.1029/2006JD007904.

Randel, W. J., F. Wu, and P. Forster (2007b), The extratropical tropopause inversion layer: Global observations with GPS data, and a radiative forcing mechanism, *J. Atmos. Sci.*, *64*, 4489–4496, doi:10.1175/2007JAS2412.1.

Randel, W. J., et al. (2009), An update of observed stratospheric temperature trends, *J. Geophys. Res.*, *114*, D02107, doi:10.1029/2008JD010421.

Rienecker, M. M., et al. (2008), The GEOS-5 data assimilation system—Documentation of versions 5.0.1, 5.1.0, and 5.2.0, *Tech. Rep. NASA, Tech. Memo., TM-2008-104606*, vol. 27, NASA, Goddard Space Flight Center, Greenbelt, Md.

Saarinen, S. (2004), *ODB User Guide*, 1st ed., ECMWF, Reading, U. K. [Available at www.ecmwf.int/research/ifsdocs/CY31r1/index.html.]

Schemm, S., H. Wernli, and L. Papritz (2013), Warm conveyor belts in idealized moist baroclinic wave simulations, *J. Atmos. Sci.*, *70*, 627–652, doi:10.1175/JAS-D-12-0147.1.

Schiemann, R., D. Luthi, and C. Schar (2009), Seasonality and interannual variability of the westerly jet in the Tibetan Plateau region, *J. Clim.*, *22*, 2940–2957.

Schmidt, T., G. Beyerle, S. Heise, J. Wickert, and M. Rothacher (2006), A climatology of multiple tropopauses derived from GPS radio occultations with CHAMP and SAC-C, *Geophys. Res. Lett.*, *33*, L04808, doi:10.1029/2005GL024600.

Shapiro, M. A. (1978), Further evidence of the mesoscale and turbulent structure of upper level jet stream-frontal zone systems, *Mon. Weather Rev.*, *106*, 1100–1110.

Shapiro, M. A. (1980), Turbulent mixing within tropopause folds as a mechanism for the exchange of chemical constituents between stratosphere and troposphere, *J. Atmos. Sci.*, *37*, 994–1004.

Shapiro, M. A., and S. G. Grønås (1999), *The Life Cycles of Extratropical Cyclones*, Am. Meteorol. Soc., Boston, Mass.

Shapiro, M. A., H. Wernli, N. A. Bond, and R. Langland (2001), The influence of the 1997-98 El Niño Southern Oscillation on extratropical baroclinic life cycles over the eastern North Pacific, *Q. J. R. Meteorol. Soc.*, *127*, 331–342, doi:10.1002/qj.49712757205.

Son, S.-W., N. F. Tandon, and M. P. Lorenzo (2011), The fine-scale structure of the global tropopause derived from COSMIC GPS radio occultation measurements, *J. Geophys. Res.*, *116*, D20113, doi:10.1029/2011JD016030.

Stohl, A., L. Haimberger, M. Scheele, and H. Wernli (2001), An intercomparison of results from three trajectory models, *Meteorol. Appl.*, *8*, 127–135.

Stohl, A., H. Wernli, P. James, M. Bourqui, C. Forster, M. A. Liniger, P. Seibert, and M. Sprenger (2003), A new perspective of stratosphere-troposphere exchange, *Bull. Am. Meteorol. Soc.*, *84*, 1565–1573.

Strong, C., and R. Davis (2006), Variability in the altitude of fast upper tropospheric winds over the Northern Hemisphere during winter, *J. Geophys. Res.*, *111*, D10106, doi:10.1029/2005JD006497.

Thorncroft, C. D., B. J. Hoskins, and M. E. McIntyre (1993), Two paradigms of baroclinic-wave life-cycle, *Q. J. R. Meteorol. Soc.*, *119*, 17–55.

Ungermann, J., et al. (2013), Filamentary structure in chemical tracer distributions near the subtropical jet following a wave breaking event, *Atmos. Chem. Phys.*, *13*, 10,517–10,534.

Wang, C. (2002), Atmospheric circulation cells associated with the EL-Niño-Southern Oscillation, *J. Clim.*, *15*, 399–419.

Wang, S., and L. M. Polvani (2011), Double tropopause formation in idealized baroclinic life cycles: The key role of an initial tropopause inversion layer, *J. Geophys. Res.*, *116*, D05108, doi:10.1029/2010JD015118.

Wernli, H., and H. C. Davies (1997), A Lagrangian-based analysis of extratropical cyclones I: The method and some applications, *Q. J. R. Meteorol. Soc.*, *123*, 467–489.

Wernli, H., and C. Schwierz (2006), Surface cyclones in the ERA-40 dataset (1958-2001). Part I: Novel identification method and global climatology, *J. Atmos. Sci.*, *63*, 2486–2507.

Wirth, V. (2001), Cyclonic/Anticyclonic asymmetry concerning the height of the thermal and the dynamical tropopause, *J. Atmos. Sci.*, *58*, 26–37.

Wirth, V. (2003), Static stability in the extratropical tropopause region, *J. Atmos. Sci.*, *60*, 1395–1409.

Wirth, V., and T. Szabo (2007), Sharpness of the extratropical tropopause in baroclinic life cycle experiments, *Geophys. Res. Lett.*, *34*, L02809, doi:10.1029/2006GL028369.

World Meteorological Organization (1957), *Meteorology: A Three-Dimensional Science: Second Session of the Commission for Aerology*, pp. 134–138, vol. 4, World Meteorol. Organ. Bull., Geneva, Switzerland.

Wright, C. J., M. B. Rivas, and J. C. Gille (2011), Intercomparisons of HIRDLS, COSMIC and SABER for the detection of stratospheric gravity waves, *Atmos. Meas. Tech.*, *4*, 1581–1591, doi:10.5194/amt-4-1581-2011.

Wright, J. S., and S. Fueglistaler (2013), Large differences in reanalyses of diabatic heating in the tropical upper troposphere and lower stratosphere, *Atmos. Chem. Phys.*, *13*, 9565–9576, doi:10.5194/acp-13-9565-2013.